To IMAGE or to IMAGINE: visualization of parasite migration as a means to support (malaria) parasite vaccine development

Korne, C.M. de


2

Quantification of wild-type and radiation attenuated *Plasmodium falciparum* sporozoite motility in human skin

Béatrice M.F. Winkel*, Clarize M. de Korne*, Matthias N. van Oosterom, Diego Staphorst, Mark Meijhuis, Els Baalbergen, Munisha S. Ganesh, Koen J. Dechering, Martijn W. Vos, Séverine C. Chevalley-Maurel, Blandine Franke-Fayard, Fijs W.B. van Leeuwen, Meta Roestenberg

**These authors contributed equally to this work*

Scientific Reports 2019. DOI: 10.1038/s41598-019-49895-3

ABSTRACT

Given the number of global malaria cases and deaths, the need for a vaccine against *Plasmodium falciparum* (*Pf*) remains pressing. Administration of live, radiation-attenuated *Pf* sporozoites can fully protect malaria-naïve individuals. Despite the fact that motility of these attenuated parasites is key to their infectivity and ultimately protective efficacy, sporozoite motility in human tissue (e.g. skin) remains wholly uncharacterized to date. We show that the ability to quantitatively address the complexity of sporozoite motility in human tissue provides an additional tool in the development of attenuated sporozoite vaccines. We imaged *Pf* movement in the skin of its natural host and compared wild-type and radiation-attenuated GFP-expressing *Pf* sporozoites. Using custom image analysis software and human skin explants we were able to quantitatively study their key motility features. This head-to-head comparison revealed that radiation attenuation impaired the capacity of sporozoites to vary their turn angle, velocity and direction, promoting less refined movement patterns. Understanding and overcoming these changes in motility will contribute to the development of an efficacious attenuated parasite malaria vaccine.

INTRODUCTION

Nearly half the human population lives in areas with an increased risk of malaria transmission, resulting in more than 200 million cases each year[1], illustrating the urgent need for a highly effective malaria vaccine. Vaccines based on live attenuated *Plasmodium falciparum* (*Pf*) parasites obtained from the mosquito salivary gland, so-called sporozoites (SPZ), are currently most promising. Clinical trials that used mosquitoes to transmit SPZ into human subjects yielded 100% protection in non-endemic settings[2-4]. When translating the seminal mosquito bite studies into a needle-based cryopreserved vaccine formulation[3], intradermal (ID) injection of isolated live attenuated SPZ were found to induce inferior protective immunity in humans[5]. Further research showed that an impractical intravenous (IV) route of attenuated SPZ injection was more effective, because IV administration promotes transportation of SPZ to the liver[3, 4, 6], which is key to the induction of protection[7, 8]. To date, the factors which affect the motility of *Pf* SPZ on their journey from human skin to liver have not been studied.

Imaging studies using genetically modified fluorescent *Plasmodium berghei (Pb*) or yoelii *(Py*) SPZ in mouse skin yielded insight into the migration patterns of SPZ, with contrasting differences between *in vitro* and *in vivo* motility or the site of injection (tail or ear)[9-14]. Because the anatomical structure of murine skin differs from human skin, with respect to thickness, muscle layers, dermal papillae and hair follicle density[15, 16], a human skin model would provide a valuable contribution. Despite differences such as the lack of blood flow, *ex vivo* skin explant models have shown excellent viability of dermal cells over long periods of time[17, 18]. Analysis of *Pf* SPZ migration in human tissue is an important first step to understanding *Pf* transmission and attenuated SPZ vaccine delivery. In addition, a human skin model could also allow for future evaluation of subunit vaccines[14].

Attenuated SPZ vaccines have been produced using radiation attenuation (RA), gene modification or concomitant drug administration[19]. RA is the most commonly used method, whereby RA SPZ vaccines are currently entering phase 3 clinical trials[20, 21]. RA introduces double strand breaks in DNA[22] and has been shown to impact the SPZ gene expression and ultrastructure[23-25]. In both ways, SPZ motility might be influenced. At present, preservation of motility following RA can only be validated using an *in vitro* gliding assay[26], where the SPZ are allowed to glide on a glass surface. However, this assay does not mimic the complexity of environmental interactions that are observed in tissue (e.g. physical confinement)[10, 27]. Therefore, *ex vivo* imaging technologies that make use of human tissue are required.

The pioneering literature that presents image analysis of rodent SPZ (*Pb*) movement in murine tissue, has focused on an often used measure of random diffusion of particles, the

mean squared displacement (MSD)[9, 10, 28]. This measurement separates anomalous diffusion (with a non-linear relation to time) from the classic linear diffusion process. This has supported quantitative investigations toward motility changes over time and in relation to dermal structures[9, 10]. As SPZ movement through tissue suits a specific purpose, it makes sense for motility analyses to include quantitative parameters for directionality rather than limit the analysis to parameters that present random diffusion. Analysis of directional movement, referred to as tortuosity, is a common approach to study e.g. animal migration through the desert[29] and analysis of disease severity in cognitively impaired patients[30], but has also been applied during cell tracking studies[31]. The tortuosity of movement indicates whether it is directional or random. We reasoned that the concept of directional movement could complement the diffusion-based in skin SPZ analysis and could provide more detailed insight in SPZ motility in complex environments such as human skin tissue.

The aim of this study was to image and quantitatively assess motility of wild-type, GFP-expressing *Pf* SPZ (Pf^{WT}) in human skin (Figure 1). For image analysis we developed a software tool for in skin analysis called $SMOOT_{human\ skin}$ (Sporozoite Motility Orienting and Organizing Tool) that can output tortuosity and velocity related motility parameters of individual *Pf* SPZ. In order to assess the effect of RA on SPZ migration, we subsequently compared the motility of Pf^{WT} and RA SPZ (Pf^{RA}) populations in human skin explants.

METHODS

Study design

In order to explore movement characteristics of *Pf* sporozoites (SPZ) in human skin explants, we performed a controlled laboratory experiment, in which we compared motility parameters (assessed using our custom software tool $SMOOT_{human\ skin}$) of 352 unattenuated *Pf* SPZ (Pf^{WT}; 14 movie sections) with those of 350 radiation attenuated *Pf* SPZ (Pf^{RA}; 18 movie sections). The movies were made of SPZ injected in human skin explants of two donors (in two independent experiments), comparing Pf^{WT} with Pf^{RA} in both donors at two different locations in the skin ending up with four unique locations for both Pf^{WT} and Pf^{RA}. The experiments were evaluated individually (Sup. Figure S1), thereafter the data was pooled (Sup. Figure S2) and the final analysis of the motility of Pf^{WT} vs Pf^{RA} was performed on the pooled dataset. The study was not randomized or blinded.

Parasites

Anopheles stephensi mosquitoes infected with a transgenic *Pf* line that constitutively expresses fluorescent reporter protein GFP under the *pf*CS promotor (NF54-ΔPf47-5'*csp*-GFP-Luc, kindly provided by dr. Koen Dechering; TropIQ Health Sciences), were killed using ethanol spray and rinsed in RPMI 1640 (Invitrogen). Salivary glands were dissected manually at day 14-21 post infection, incubated in RPMI 1640 and kept on ice. Radiation attenuation

of SPZ was performed by irradiating intact salivary glands to a total dose of 20 krad using a Cesium radiation source (total of 28 minutes) on ice. During this time control SPZ were also kept on ice. Within 1 hr, glands were homogenized to release *Pf* SPZ. SPZ were then counted using a Bürker counting chamber, brought to a concentration of 20 x 10^6/ml in RPMI 1640 containing 10% Fetal Calf Serum (FCS; Bodinco) and used for imaging experiments immediately.

Skin explants

We obtained human skin explants from collaborating hospitals immediately after abdominal skin reduction surgery. The use of human skin explants for this research was approved by the Commission Medical Ethics (CME) of the LUMC (CME: B18-009). The methods were carried out in accordance with the relevant guidelines and regulations, and informed consent was obtained from all participants. The skin explants were kept at 4°C for 3 hr until use. Subcutaneous fat was removed and the epidermal side was cleaned with 70% ethanol. One million SPZ were injected intradermally in a 50 µl injection using a 0.3 ml insulin syringe (30G; BD). In order to facilitate quick localization of the injection site by confocal microscopy the injection formulation contained Yellow-Green fluorescent 500 nm Latex nanoparticles (Sigma Aldrich). Immediately after injection, the injection site was biopsied using a 6 mm biopsy punch, sliced longitudinally through the center and mounted on a microscopy slide with a 1 mm depression in RPMI 10% FCS. Slides were imaged within 30 minutes post injection.

Confocal imaging

Skin biopsy slides were imaged using the time-lapse function of the Leica TSC (true confocal scanning) SP8 microscope (Leica Microsystems). 2D images (no z-stacks) were obtained using an exposure time of 1.7 seconds per frame (400 frames per movie section, 11 minutes) and a 40x objective. Microscopy videos were rendered using accompanying Leica LASX software and were analyzed using custom software $SMOOT_{human\ skin}$.

Movie analysis with $SMOOT_{human\ skin}$

MATLAB (The MathWorks Inc. Natick, MA, USA) software was created for in skin SPZ analysis, which we called Sporozoite Motility Orienting and Organizing Tool ($SMOOT_{human\ skin}$). This tool is an extended version compared to the $SMOOT_{human\ skin}$ tool previously used to determine the velocity and movement pattern distribution of $Cy5M_2$ labeled *Pf* SPZ[32]. Similar to our recently published *in vitro* tool $SMOOT_{in\ vitro}$[33], the upgraded $SMOOT_{human\ skin}$ software now also includes turn angle and displacement. In addition, $SMOOT_{human\ skin}$ takes into account the directionality by computing the angular dispersion, straightness index and the direction of SPZ tracks. Firstly, SPZ tracks were characterized as motile or stationary based on their displacement. Subsequently, motile tracks were subdivided into movement patterns: sharp

turn, slight turn and linear.

To investigate the influence of RA on SPZ motility, we compared $SMOOT_{human\ skin}$ parameter outcomes of 14 *Pf*^{WT} motility movie files (11 minutes/movie, 154 minutes total, 352 SPZ tracks consisting of 511 segments and 26932 frames; Sup. Movie S1) with 18 *Pf*^{RA} motility files (11 minutes/ movie, 198 minutes total, 350 SPZ tracks consisting of 563 segments and 25804 frames; Sup. Movie S2). Software output was manually validated.

Velocity was determined by measuring the displacement between frames. We defined step number in the track *i* to measure velocity *v* using formula (1), with *x as* the median pixel location of the segmented structure and *t* as the time passed in seconds.

(1) $$v(i) = \frac{x_i - x_{i-1}}{t_i - t_{i-1}} = \frac{dx}{dt}$$

The mean squared displacement (MSD) is a common measure to distinguish random versus non-random motion for moving particles and was previously used to analyze SPZ motility[9, 10]. The squared displacement (SD) is a measure of the displacement per time point of an individual track, which can be calculated with formula (2):

(2) $$SD(i) = \big(x_n(i) - x_n(0)\big)^2$$

The MSD was derived from the SD of all linear tracks using formula (3):

(3) $$MSD(i) = \langle (x(i) - x_0)^2 \rangle = \frac{1}{N}\sum_{n=1}^{N} \big(x_n(i) - x_n(0)\big)^2$$

The turn angle (θ) of the SPZ was defined by the angle difference between path directions in consecutive frames. If we start calculating the turn angle from location x_0 then the SPZ reaches x_i after *i* steps. The angle of x_i is the angle δ_i between point x_i and the horizontal. The turn angle was then defined as described in formula (4).

(4) $$\theta_i = \delta_i - \delta_{i-1}$$

The straightness index (SI) is the most basic approach to quantify tortuosity and is defined as the ratio of distance between track end points (*C*) and track length (*L*), as calculated using formula (5). This parameter quantifies deviation from a straight line, e.g. SI = 1 means a

perfect linear path, SI = 0 means circular motion.

(5) $$SI = \frac{C_{track}}{L_{track}} = \frac{x(i) - x(0)}{\sum_{k=1}^{i}\big(x(k) - x(k-1)\big)}$$

Angular dispersion (AD) quantifies the number of turning angles diverging from the main angle of movement. It describes tortuosity by quantifying changes in direction. It is calculated using the turn angles (formula (4)) according to the following formula:

(6) $$AD = \frac{1}{I}\sqrt{C^2 + S^2}$$

Where I is the last step of the track and C and S are defined as:

(7) $$C = \sum_{i=1}^{I} \cos\theta_i \;\; S = \sum_{i=1}^{I} \sin\theta_i$$

Statistics

Data extracted from $SMOOT_{human\ skin}$ was analyzed in IBM (Armonk, NY, USA) SPSS version 23 or GraphPad Prism (La Jolla, CA, USA) version 7. Comparisons between two or more independent categorical data groups were made by Chi-squared test, continuous nonparametric parameters were compared by Mann-Whitney U test. P<0.05 was considered statistically significant. Bonferroni correction was applied for post hoc analysis after Chi-squared testing.

RESULTS

Generation of a semi-automated sporozoite migration analysis tool

Firstly, we generated confocal microscopy movies of Pf^{WT} and Pf^{RA} migrating through human skin explants by a trans sectional skin setup (fourteen 11 min movie sections of Pf^{WT} and eighteen 11 min movie sections of $Pf^{RA,}$ yielding a total of 352 and 350 analyzed SPZ, respectively). Experiments were performed in two independent donor samples and while splitting the batch of SPZ in a Pf^{WT} and Pf^{RA} group. Using our semi-automated software tool $SMOOT_{human\ skin}$, we were able to track SPZ movement (Figure 1) by identifying SPZ based on their shape and fluorescence intensity (Figure 1B) and connecting their location over time (see Sup. Figure S1 for an overview of the data per individual location and supplementary movie S1 and S2 for examples). SPZ locations per frame were stitched together in order to

generate track segments, where multiple segments in the same 2D plane build up a full track (Figure 1B-C). Depending on the straightness index (SI) of the individual segments, their movement patterns (sharp turn, slight turn and linear) were determined and color-coded (Figure 1C). Slight turns were defined as the turns which resulted from the natural curvature of the SPZ (0.21-0.23 μm^{-1})[34].

Sharper turns, requiring extra bending of the SPZ, were defined as sharp turns[34]. Furthermore, the following movement parameters were calculated at track level: straightness index (SI) and angular dispersion (AD), at segment level: turn direction (clockwise or counter clockwise) and at frame level: mean squared displacement (MSD) and velocity. Using the unique ID allocated to each individual SPZ track, all computed parameters were extracted for the individual SPZ and, where relevant, analyzed over time. In the experiments 81% of the SPZ were characterized as motile, which surpasses the 66% reported earlier for *Pb* SPZ in murine skin[9].

Mean Squared Displacement (MSD) data alone does not reflect individual sporozoite movement heterogeneity

In analogy to previous protocols for *Pb* SPZ[10], we evaluated the MSD of linear Pf^{WT} tracks (37% of tracks). Comparing the MSD of Pf^{WT} with the Pf^{RA} population (containing 18.5% total linear tracks) yielded no significant difference (Figure 2A). This analysis, however, excluded a large fraction of SPZ that exhibited non-linear movement (slight and sharp turn; 81.5% for Pf^{RA} and 63% for Pf^{WT}). We thus concluded that this analysis methodology was not suitable to fully grasp the complexity of *Pf* motility in human skin. In addition, we found that squared displacement plots of SPZ revealed a high level of heterogeneity. A typical example of this heterogeneity is shown in Figure 2B-C, where we plotted the squared displacement (SD; where displacement is the difference in SPZ position between begin and endpoint of a track) of 4 very different individual SPZ tracks from the same movie file. In order to do justice to the sample heterogeneity, we aimed to include other parameters of movement, such as the tortuosity, in the motility analysis.

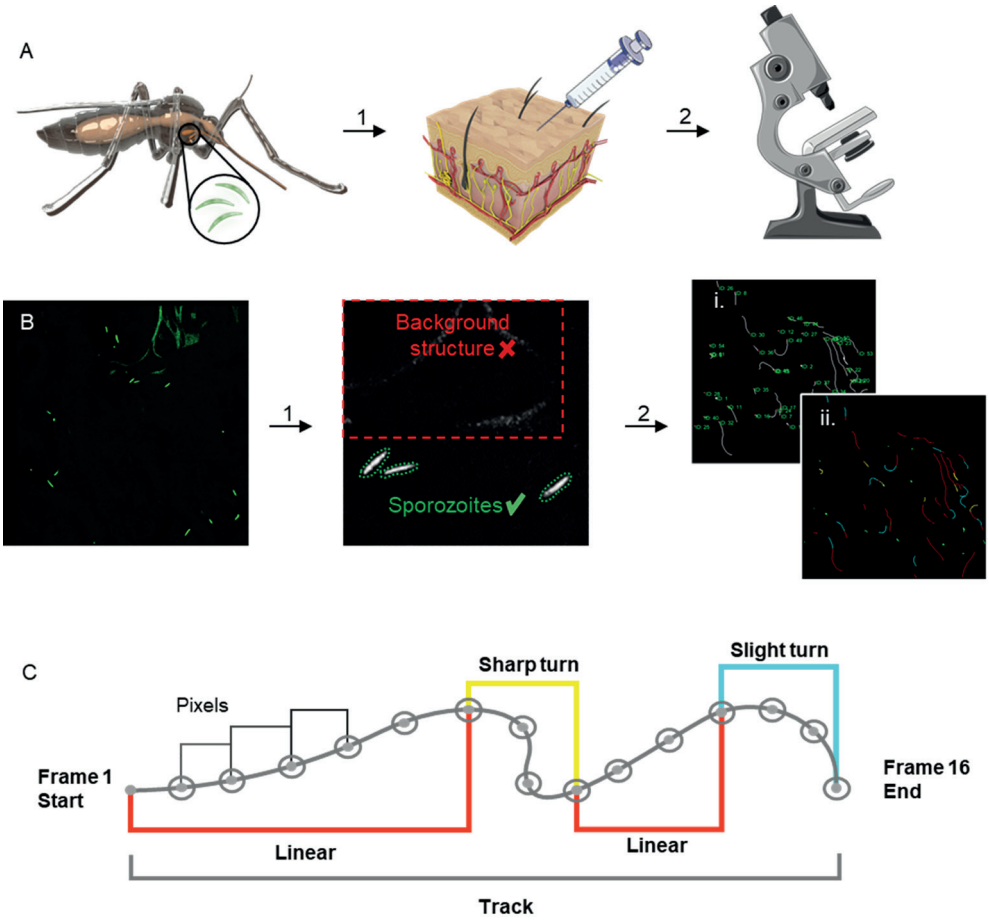

Figure 1 Schematic of experimental setup and SMOOT$_{\text{human skin}}$ analysis. A) Schematic of an *Anopheles* mosquito as the host of *Plasmodium* SPZ within its salivary glands. Isolated SPZ, *Pf*$^{\text{WT}}$ or *Pf*$^{\text{RA}}$, were injected into human skin (1). The skin samples containing SPZ were filmed using a confocal microscope (2) (Images of needle and microscope were adapted from image copyright https://smart.servier.com, Creative Commons Attribution 3.0 Unported License, https://creativecommons.org/licenses/by/3.0/). B) Raw confocal video images were uploaded into SMOOT$_{\text{human skin}}$. Per video frame individual SPZ were semi-automatically segmented (1). Segmented SPZ in consecutive frames were stitched to generate tracks. Generated tracks have a unique SPZ ID (i) in order to extract measured parameters (for example movement pattern (ii)) per SPZ over time (2). C. SPZ tracks are divided into segments based on the underlying movement pattern.

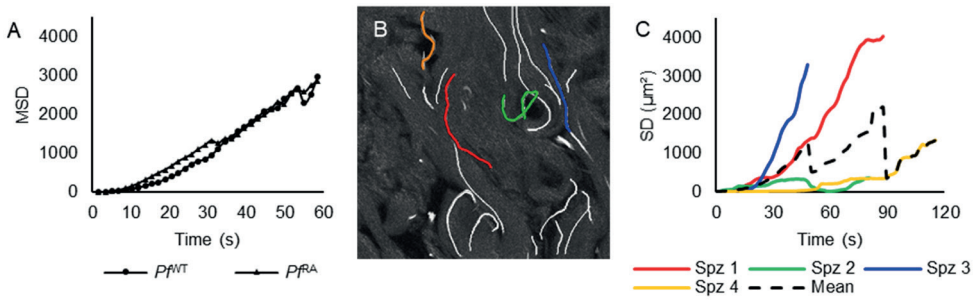

Figure 2 Mean squared displacement of sporozoites. A) Mean squared displacement (MSD in µm^2) of the SPZ plotted against time, only linear tracks are taken into account. B) Examples of individual SPZ tracks in a single movie file. C) The four differently colored individual tracks from B. are presented as squared displacement (SD in µm^2) over time and presented relative to the dotted line, which presents the MSD of all four lines.

Tortuosity analysis reveals differences in sporozoite motility after RA

Using tortuosity-based analysis we quantified pattern characteristics of SPZ tracks. First, the individual experiments were evaluated (Sup. Figure S1), thereafter the data of all *Pf*^{RA} and *Pf*^{WT} was pooled (Sup. Figure S2) and further analyzed. Automated pattern classification of SPZ tracks showed that 37% of *Pf*^{WT} tracks were linear, 42% classified as sharp turn and 21% as slight turn (Fig. 3A). *Pf*^{WT} tracks displayed a median SI of 0.86, indicating relatively straight tracks (SI close to 1 indicates a linear track; Figure 3B) and a balanced AD of 0.45 indicating random meandering of SPZ (AD close to 1 indicates a consistent track, AD close to 0 indicate random direction changes; Figure 3C).

In contrast, the *Pf*^{RA} population displayed significantly more slight and sharp turn segments (7.2% blue and 74.3% yellow color coding respectively), and a decrease in linear patterns (18.5%, red) as compared to the *Pf*^{WT} (Figure 3A). This difference was caused by continuous circular turning behavior of SPZ (arrowheads Figure 3A), as well as a back and forth motion (180° turn; hereafter termed 'reversal'). Although *in vitro* on circular movement of *Pf* is reported on coated surfaces, under the conditions studied, *Pf* did not show such movement (see Sup. Movie S4). This was confirmed by an increase in SI values close to 0, representing these turning tracks (Figure 3B; post hoc Chi squared test p=0.008 and p=<0.0001 respectively). In addition, *Pf*^{RA} showed significantly more persistent straight tracks compared to *Pf*^{WT} (increased indices close to 1; overall Chi squared test p=<0.0001; median SI 0.89). Similarly, *Pf*^{RA} showed more consistent tracks with fewer deviations from the mean angle of movement patterns compared to *Pf*^{WT} (Figure 3C; angular dispersion median 0.92; overall Chi squared test p=<0.001 post hoc Chi squared test AD >0.75 p=<0.0001). Taken together, the pattern analysis and tortuosity parameters indicate that *Pf*^{RA} exhibit reduced motility variation compared to *Pf*^{WT} and preferentially display continuous circling patterns.

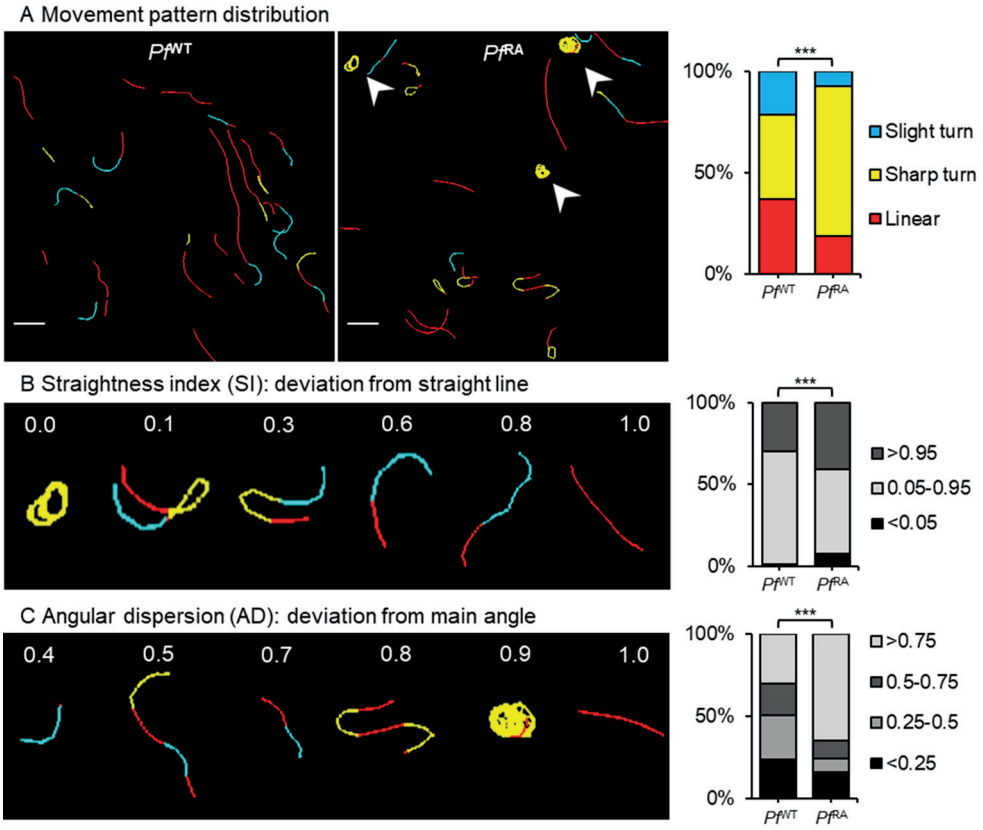

Figure 3 Tortuosity of sporozoite tracks. A) Two examples of movement pattern maps of tracked SPZ; *Pf*^{WT} in skin (left) and *Pf*^{RA} in skin (middle). Linear segments are depicted in red, slight turns in blue and sharp turns in yellow. Arrowheads indicate circular SPZ tracks comparable to *in vitro* movement. The movement pattern distribution of the *Pf*^{WT} and *Pf*^{RA} is quantified for all SPZ tracks based on frames (right). Scale bar: 20 µm. B) To illustrate the concept of straightness index (SI) in relation to SPZ tracks, 6 tracks are displayed out of the movement pattern maps shown in A. The SI distribution is quantified based on the SI values of total tracks (*Pf*^{WT} median: 0.89, IQR: 0.66-0.96; *Pf*^{RA} median: 0.90, IQR: 0.46-0.98). C) To illustrate the concept of angular dispersion (AD) in relation to SPZ tracks, 6 tracks are displayed out of the movement pattern maps shown in A. The AD distribution is quantified based on the AD values of total tracks (*Pf*^{WT} median: 0.47, IQR: 0.26-0.80; *Pf*^{RA} median: 0.93, IQR: 0.51-0.99). *** = p<0.0001 using Chi squared test.

RA causes sporozoites to circle consistently in a clockwise direction

Possibly due to the tilted arrangement of the SPZ polar-ring[35], circularly moving SPZ display a preferred clockwise (CW) turn direction *in vitro*[36]. In the three dimensional (3D) skin environment this preference was lost; $SMOOT_{human\ skin}$ analysis demonstrated that *Pf*^{WT} turned equally CW and counterclockwise (CCW; Figure 4A). Surprisingly, analysis of turn direction in the *Pf*^{RA} population yielded a preference for CW directionality (Figure 4A; 65.2% CW; p=0.013). Analysis of the duration of the turns (number of frames) revealed that *Pf*^{RA}

continued turning in circles when this pattern was initiated.

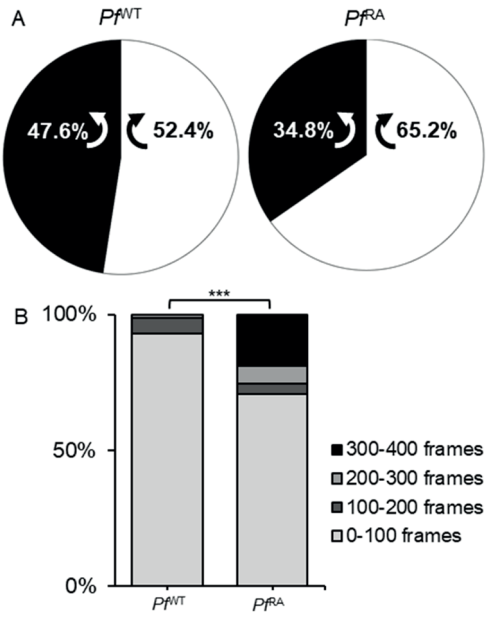

Figure 4 Direction of turning sporozoites. A) Turn direction of *Pf*^{WT} and *Pf*^{RA} in skin. *Pf*^{RA} turn significantly more CW than *Pf*^{WT}, p=0.013 using Chi-Squared test. B) The sharp turns of *Pf*^{RA} contain significantly more frames than the turns of *Pf*^{WT} (*Pf*^{WT} median: 32, IQR: 22-55; *Pf*^{RA} median: 33, IQR: 14-218; p>0.000 using Chi-Squared test). Indicating persistent circular motion.

Per frame analysis of velocity reveals decreased velocity alterations after RA

In line with previous findings[9, 10, 37], we recorded an average SPZ velocity per track of 1.1 µm/s (time did not seem to have an effect on the average velocity (Sup. Figure S3)). $SMOOT_{human\ skin}$ also allowed analysis of the velocity per captured frame within a track (Figure 5), revealing marked variations over time. Examples illustrate that a single SPZ could display non-parametric velocity changes between 0 and 3.5 µm/s over the course of one track (Figure 5A). While the velocity changes occurred within all movement patterns, the median velocity was highest in linear segments followed by slight turns and in sharp turns (Figure 5B). *Pf*^{RA} consistently showed higher velocity in all movement patterns (median 1.1 µm/s vs 0.85 µm/s for linear tracks, 0.6 vs 0.48 µm/s for slight turns and 0.34 vs 0.24 µm/s for sharp turns in *Pf*^{RA} vs *Pf*^{WT} respectively, p=<0.0001). Despite the fact that *Pf*^{RA} displayed more 'slow' sharp turns, in a per frame analysis their overall median velocity at 0.37 µm/s was higher than the median velocity of *Pf*^{WT} (0.35 µm/s; p=<0.0001). This difference was caused by a reduction in stop-and-go action (frames with velocity <0.5 µm/s were 56.8 % for *Pf*^{RA} and 59.6 % for *Pf*^{WT}, p=0.037). Furthermore, velocity variability was smaller in *Pf*^{RA}

(Figure 5B, range 0-4.1 µm/s) compared to Pf^{WT} (0-4.8 µm/s). Corroborating this finding, Pf^{RA} velocities of linear tracks were normally distributed compared to a nonparametric velocity distribution for Pf^{WT} (Figure 5B, p=<0.0001), whereas velocities in other movement patterns were nonparametrically distributed for both Pf^{RA} and Pf^{WT}. Taken together, Pf^{RA} less readily alternated their velocity.

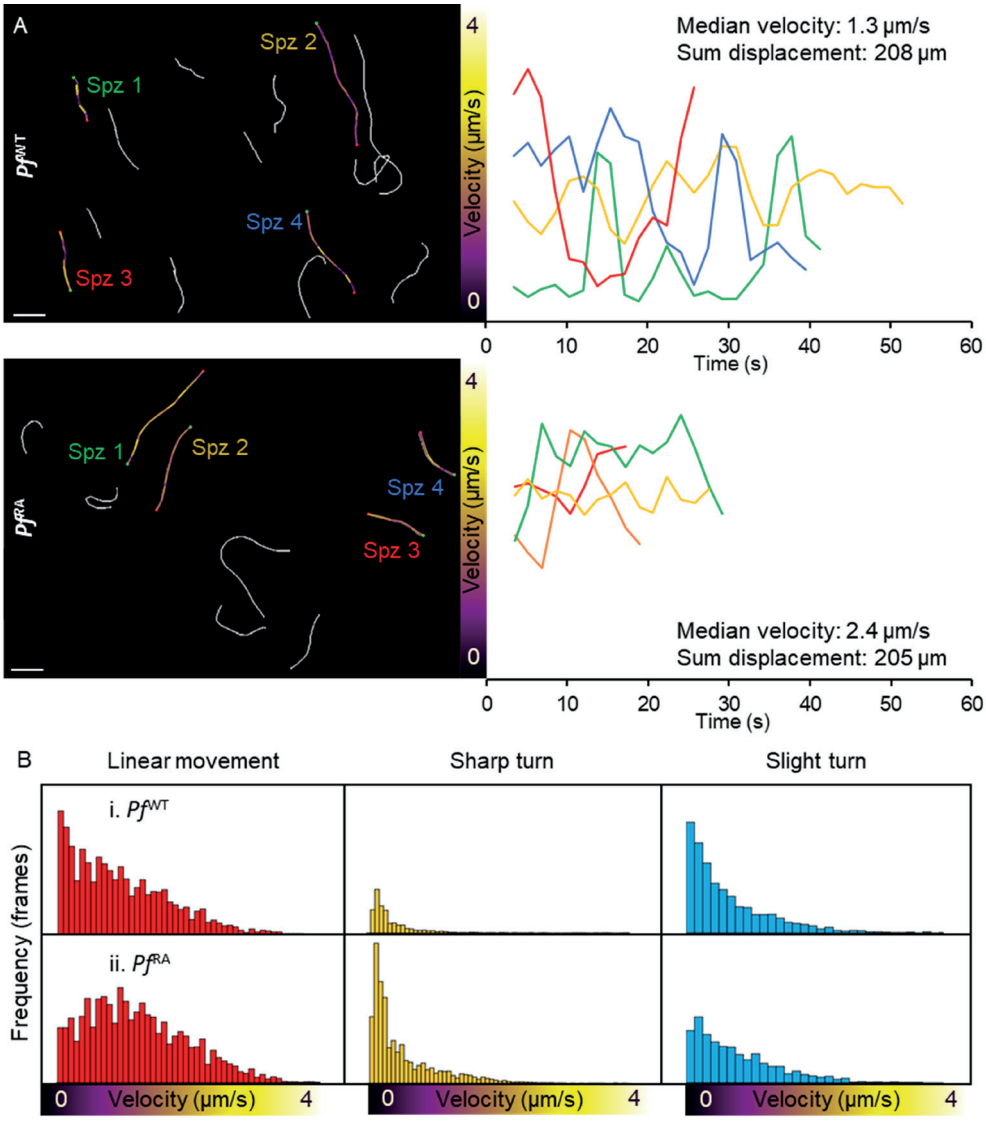

Figure 5 Velocity of sporozoites. A) Four Pf^{WT} (above) and four Pf^{RA} (below) tracks are color-coded based on velocity. Scalebar: 20 µm. Their individual velocity is plotted over time (right). B) Velocity distribution of Pf^{WT} and Pf^{RA} per movement pattern.

***Pf*^{RA} display a default motility pattern: reversal**

Interestingly, some SPZ in the *Pf*^{RA} group (9% of motile *Pf*^{RA} tracks) revealed pendulum movement, whereby they reverse direction repeatedly moving up and down a short path (Figure 6; Sup. Movie S3). This is in line with earlier findings where SPZ moved in this particular fashion while residing in the mosquito[38-40]. Plotting this movement (over x and y axis) over time yielded a sinuous track (yellow) that is clearly distinct from the short linear track (red) observed in the same movie segment. Strikingly, this movement pattern was not observed in *Pf*^{WT}.

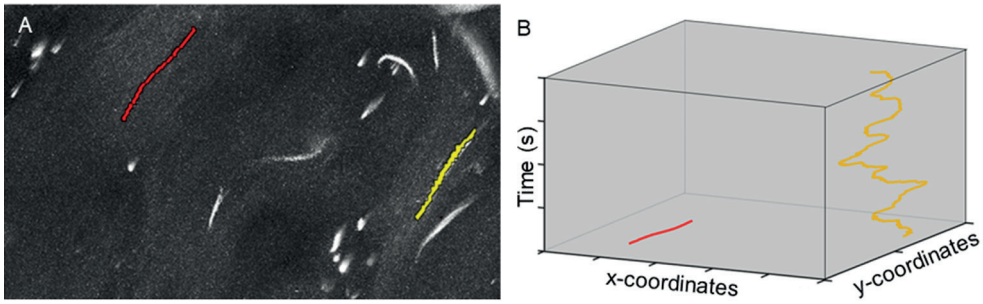

Figure 6 Reverse movement. A) In this example, one SPZ was moving in a linear direction and one SPZ was moving back and forth. The linear track is depicted in red, the reverse movement is classified as a sharp turn, thereby depicted in yellow. B) The coordinates of the linear and the reversal track are plotted in a xyt coordinate axis system.

DISCUSSION

In this study we compared movement of wild-type with irradiated *Pf* SPZ in a human skin explant using our semi-automated custom analysis tool for SPZ tracking. We found that *Pf*^{RA} display increased circular motility patterns, more extreme SI values and higher AD compared to *Pf*^{WT}. In addition, *Pf*^{RA} exhibited less variability in velocity over the course of their track and 'reversal' patterns were unique to this group. Combined, the data indicates that attenuation via radiation may alter SPZ motility.

In vitro, SPZ display very elementary circular movement with little variation in velocity, angle or direction[36, 41, 42]. Recently, we reported that for *Pb* SPZ, a complex interplay of various nutrients including albumin, glucose and certain amino acids and vitamins regulates parasite motility *in vitro*[33]. Under the conditions used to study the movement in human skin explants (uncoated glass; RPMI 160 + 10% FCS) *Pf* SPZ did not display this movement pattern *in vitro* (Sup. Movie S4). In skin, however, sharp turns (combination of circular and reversal movement) were observed in addition to linear and slight turn movement patterns. This indicates that the environment influences *Pf* SPZ movement and in particular

their directionality. It was previously shown for *Pb* SPZ that an environment with artificial physical constraints in the form of pillars increases the movement directionality as function of interstitial space[27]. This trend is in line with the reported increase of tortuosity in porous materials that occurs when reducing the interstitial space[43]. An influence of tissue structure on directionality of *Pb* SPZ can also be extrapolated from the different motility patterns in the skin of mouse ears as compared to the skin of a mouse tail[10]. Our findings suggest that the highly complex heterogeneity of human skin composition, in combination with the mixed nutrient availability, may similarly impact motility patterns of individual SPZ, generating highly complex movement patterns which vary according to the local donor tissue structure.

Although *Pf* SPZ displayed average track velocities in line with previous reports (on average 1.1 µm/s as compared to previous studies reporting averages of 0.9-1.5 µm/s in mouse skin[9, 10, 37]), a per frame velocity analysis revealed ongoing stop-and-go actions. These heterogeneous patterns in combination with the high level of path tortuosity suggest that environmental cues and cellular interactions such as traversal[44] impact heterogeneity of direction and speed of the SPZ. Indeed, the SPZ surface displays many proteins such as CSP, SPECT1 and CelTOS which facilitate interaction with targets like heparan sulphate and αvβ3 integrin which are present in human skin[11, 45, 46]. Because these alterations in velocity resulted in a nonparametric velocity distribution, that differs between SPZ taking sharp or slight turns or moving straight, we reason that average velocity alone is insufficient to unravel complex migratory behavior.

Our findings suggest that radiation may not only effectively attenuate *Pf* SPZ at the liver stage, which has been described before[8], but could also influence their motility at the skin stage. Similar to what has been described before with respect to the effect of cryopreservation on *Pb* SPZ motility[47], RA also seems to induce small alterations in motility. The differences in motility between Pf^{WT} and Pf^{RA} (observed in samples from both donors), although minor, are indicative of a reduced complexity of the Pf^{RA} interaction with the tissue environment. Moreover, the increased AD of Pf^{RA}, and the increased duration of their turns seems to suggest that once a 'default' movement pattern has been initiated, the movement pattern persists. Since circling and reversal patterns result in Pf SPZ remaining in a single location, one could argue that this movement pattern would render SPZ at risk for elimination by phagocytic dermal immune cells, which could impact antigen presentation and vaccine efficacy.

Understanding how radiation attenuation interferes with these pathogen-host interactions could be important to identify novel vaccine targets or improve the efficacy of existing radiation attenuated SPZ vaccines. Here it should be noted that for our studies we solely

used 20 krad attenuation dose as described previously in murine studies[48, 49], meaning we cannot state if a similar difference would be observed at lower radiation doses. However, increased radiation dosages result in reduced infectivity of *Plasmodium* species and reduced effectivity of attenuated parasite immunization[8, 50]. The altered motility induced by radiation may contribute to this reduced infectivity. It remains to be investigated whether similar effects also occur when using genetically modified SPZ vaccines[51-53].

Using viable human skin explants allowed us to analyze *Pf* SPZ movement in their natural skin environment thereby enhancing the possibilities to gain insight in their behavior. Obviously, also this model system has limitations. Although not per se relevant for the field of live attenuated *Pf* vaccines, intradermal syringe-based injections may not accurately represent the mosquito-based transmission of the disease[54]. The lack of blood and lymphatic circulation prevents *Pf* to migrate out of the skin, which means the motility of the total population of administered *Pf* is analyzed. Due to light attenuation in tissue, the analysis of SPZ movement was restricted to 2D, which shortened the length of the more linear tracks and thus biased circular and reversal movement patterns occurring in plane. Finally, the location in the dermis that was imaged seemed to affect SPZ movement patterns, even when the same batch of *Pf* was used. Nevertheless, we feel confident that the analysis performed in *ex vivo* human skin helps building a bridge between *in vitro* assays and *in vivo* assays of *Pb* SPZ in mouse skin[9, 10] and controlled human infection studies[21, 51].

In conclusion, we imaged *Pf* SPZ migration in the dermis of their natural host and performed an in-depth analysis of the motility of wild-type and irradiated *Pf* SPZ. We demonstrate loss of movement variability after radiation attenuation which might reflect reduced viability and ultimately decreased infectivity. Because of the ability of $SMOOT_{human\ skin}$ to analyze complex migration, it may contribute to the refinement of live SPZ vaccine formulations.

Acknowledgments: The authors would like to thank Sven van Leeuwen for his contribution to the images in this article. The research leading to these results has received funding from a ZONMW VENI grant (016.156.076) financed by the Netherlands Organization for Scientific Research (NWO) and a Gisela Thier fellowship of the LUMC.

REFERENCES

1. Organization, W.H., World malaria report 2018. World Health Organization: Geneva, 2018.
2. Roestenberg, M., et al., Protection against a malaria challenge by sporozoite inoculation. N Engl J Med, 2009. 361(5): p. 468-77.
3. Seder, R.A., et al., Protection against malaria by intravenous immunization with a nonreplicating sporozoite vaccine. Science, 2013. 341(6152): p. 1359-65.
4. Ishizuka, A.S., et al., Protection against malaria at 1 year and immune correlates following PfSPZ vaccination. Nat Med, 2016. 22(6): p. 614-23.
5. Epstein, J.E., et al., Live attenuated malaria vaccine designed to protect through hepatic CD8(+) T cell immunity. Science, 2011. 334(6055): p. 475-80.
6. Mordmuller, B., et al., Sterile protection against human malaria by chemoattenuated PfSPZ vaccine. Nature, 2017. 542(7642): p. 445-449.
7. Cochrane, A.H., R.S. Nussenzweig, and E.H. Nardin, Immunization against sporozoites. Malaria in Man and Experimental Animals, 1980: p. Academic Press, New York, Editor: Kreier, J.P. Pages 163-202.
8. Silvie, O., et al., Effects of irradiation on Plasmodium falciparum sporozoite hepatic development: implications for the design of pre-erythrocytic malaria vaccines. Parasite Immunol, 2002. 24(4): p. 221-3.
9. Hopp, C.S., et al., Longitudinal analysis of Plasmodium sporozoite motility in the dermis reveals component of blood vessel recognition. Elife, 2015. 4.
10. Hellmann, J.K., et al., Environmental constraints guide migration of malaria parasites during transmission. PLoS Pathog, 2011. 7(6): p. e1002080.
11. Amino, R., et al., Quantitative imaging of Plasmodium transmission from mosquito to mammal. Nat Med, 2006. 12(2): p. 220-4.
12. Vanderberg, J.P. and U. Frevert, Intravital microscopy demonstrating antibody-mediated immobilisation of Plasmodium berghei sporozoites injected into skin by mosquitoes. Int J Parasitol, 2004. 34(9): p. 991-6.
13. Douglas, R.G., et al., Screening for potential prophylactics targeting sporozoite motility through the skin. Malar J, 2018. 17(1): p. 319.
14. Aliprandini, E., et al., Cytotoxic anti-circumsporozoite antibodies target malaria sporozoites in the host skin. Nature Microbiology, 2018. 3(11): p. 1224-1233.
15. Pasparakis, M., I. Haase, and F.O. Nestle, Mechanisms regulating skin immunity and inflammation. Nat Rev Immunol, 2014. 14(5): p. 289-301.
16. Treuting, P.M., S.M. Dintzis, and K.S. Montine, Comparative Anatomy and Histology: A Mouse and Human Atlas. Academic Press, Elsevier, 2017. Chapter 24: p. 433-441.
17. Frade, M.A., et al., Prolonged viability of human organotypic skin explant in culture method (hOSEC). An Bras Dermatol, 2015. 90(3): p. 347-50.
18. Gunawan, M., L. Jardine, and M. Haniffa, Isolation of Human Skin Dendritic Cell Subsets. Methods Mol Biol, 2016. 1423: p. 119-28.
19. Menard, R., et al., Looking under the skin: the first steps in malarial infection and immunity. Nat Rev Microbiol, 2013. 11(10): p. 701-12.
20. Richie, T.L., et al., Progress with Plasmodium falciparum sporozoite (PfSPZ)-based malaria vaccines. Vaccine, 2015. 33(52): p. 7452-61.
21. Hoffman, S.L., et al., Protection of humans against malaria by immunization with radiation-attenuated Plasmodium falciparum sporozoites. J Infect Dis, 2002. 185(8): p. 1155-64.
22. Jeggo, P.A. and M. Lobrich, DNA double-strand breaks: their cellular and clinical impact? Oncogene, 2007. 26(56): p. 7717-9.
23. Oakley, M.S., et al., Molecular Markers of Radiation Induced Attenuation in Intrahepatic Plasmodium falciparum Parasites. PLoS One, 2016. 11(12): p. e0166814.
24. Hoffman, B.U. and R. Chattopadhyay, Plasmodium falciparum: effect of radiation on levels of gene transcripts in sporozoites. Exp Parasitol, 2008. 118(2): p. 247-52.
25. Singer, M., et al., Zinc finger nuclease-based double-strand breaks attenuate malaria parasites and reveal rare microhomology-mediated end joining. Genome Biol, 2015. 16: p. 249.
26. Prinz, H.L., J.M. Sattler, and F. Frischknecht, Plasmodium Sporozoite Motility on Flat Substrates. .

Bio-protocol, 2017. 7(14): p. e2395.
27. Battista, A., F. Frischknecht, and U.S. Schwarz, Geometrical model for malaria parasite migration in structured environments. Phys Rev E Stat Nonlin Soft Matter Phys, 2014. 90(4): p. 042720.
28. Beltman, J.B., A.F. Maree, and R.J. de Boer, Analysing immune cell migration. Nat Rev Immunol, 2009. 9(11): p. 789-98.
29. Miller, C., M.C. Christman, and I. Estevez, Movement in a condifed space: Estrimating path tortuosity. Applied Animal Behaviour Science, 2011(135): p. 13-23.
30. Kearns, W.D., J.L. Fozard, and V.O. Nams, Movement Path Tortuosity in Free Ambulation: Relationships to Age and Brain Disease. IEEE J Biomed Health Inform, 2017. 21(2): p. 539-548.
31. Loosley, A.J., et al., Describing directional cell migration with a characteristic directionality time. PLoS One, 2015. 10(5): p. e0127425.
32. Winkel, B.M.F., et al., A tracer-based method enables tracking of Plasmodium falciparum malaria parasites during human skin infection. Theranostics, 2019. 9(10): p. 2768-2778.
33. de Korne, C.M., et al., Regulation of Plasmodium sporozoite motility by formulation components. Malar J, 2019. 18(1): p. 155.
34. Muthinja, M.J., et al., Microstructured Blood Vessel Surrogates Reveal Structural Tropism of Motile Malaria Parasites. Adv Healthc Mater, 2017. 6(6).
35. Kudryashev, M., et al., Structural basis for chirality and directional motility of Plasmodium sporozoites. Cell Microbiol, 2012. 14(11): p. 1757-68.
36. Vanderberg, J.P., Studies on the motility of Plasmodium sporozoites. J Protozool, 1974. 21(4): p. 527-37.
37. Amino, R., et al., Imaging malaria sporozoites in the dermis of the mammalian host. Nat Protoc, 2007. 2(7): p. 1705-12.
38. Quadt, K.A., et al., Coupling of Retrograde Flow to Force Production During Malaria Parasite Migration. ACS Nano, 2016. 10(2): p. 2091-102.
39. Frischknecht, F., et al., Imaging movement of malaria parasites during transmission by Anopheles mosquitoes. Cell Microbiol, 2004. 6(7): p. 687-94.
40. Munter, S., et al., Plasmodium sporozoite motility is modulated by the turnover of discrete adhesion sites. Cell Host Microbe, 2009. 6(6): p. 551-62.
41. Yoeli, M., Movement of the Sporozoites of Plasmodium Berghei (Vincke Et Lips, 1948). Nature, 1964. 201: p. 1344-5.
42. Stewart, M.J. and J.P. Vanderberg, Malaria sporozoites leave behind trails of circumsporozoite protein during gliding motility. J Protozool, 1988. 35(3): p. 389-93.
43. Pisani, L., Simple Expression for the Tortuosity of Porous Media. Transp Porous Med, 2011(88): p. 193-203.
44. Amino, R., et al., Host cell traversal is important for progression of the malaria parasite through the dermis to the liver. Cell Host Microbe, 2008. 3(2): p. 88-96.
45. Coppi, A., et al., The malaria circumsporozoite protein has two functional domains, each with distinct roles as sporozoites journey from mosquito to mammalian host. J Exp Med, 2011. 208(2): p. 341-56.
46. Dundas, K., et al., Alpha-v-containing integrins are host receptors for the Plasmodium falciparum sporozoite surface protein, TRAP. Proc Natl Acad Sci U S A, 2018. 115(17): p. 4477-4482.
47. Prinz, H., et al., Immunization efficacy of cryopreserved genetically attenuated Plasmodium berghei sporozoites. Parasitology Research, 2018. 117(8): p. 2487-2497.
48. Hafalla, J.C., et al., Short-term antigen presentation and single clonal burst limit the magnitude of the CD8(+) T cell responses to malaria liver stages. Proc Natl Acad Sci U S A, 2002. 99(18): p. 11819-24.
49. Ocana-Morgner, C., M.M. Mota, and A. Rodriguez, Malaria blood stage suppression of liver stage immunity by dendritic cells. J Exp Med, 2003. 197(2): p. 143-51.
50. Mellouk, S., et al., Protection against malaria induced by irradiated sporozoites. Lancet, 1990. 335(8691): p. 721.
51. Roestenberg, M., et al., Controlled human malaria infections by intradermal injection of cryopreserved Plasmodium falciparum sporozoites. Am J Trop Med Hyg, 2013. 88(1): p. 5-13.
52. Belnoue, E., et al., Protective T cell immunity against malaria liver stage after vaccination with live sporozoites under chloroquine treatment. J Immunol, 2004. 172(4): p. 2487-95.

53. Mueller, A.K., et al., Genetically modified Plasmodium parasites as a protective experimental malaria vaccine. Nature, 2005. 433(7022): p. 164-7.
54. Haeberlein, S., et al., Protective immunity differs between routes of administration of attenuated malaria parasites independent of parasite liver load. Sci Rep, 2017. 7(1): p. 10372.

SUPPLEMENTARY INFORMATION

Evaluation and pooling of individual experiments

Two independent experiments were performed to investigate the effect of radiation attenuation on SPZ motility. During each experiment SPZ were obtained by dissection and half of them were radiated to obtain a Pf^{WT} and Pf^{RA} sample. One million Pf^{WT} and Pf^{RA} were injected intradermally in a skin explant from the same donor and imaged by confocal microscopy, both samples at two different locations. The movies made at the 4 different locations per donor were divided in sections of 400 frames, because the length of the movies varied from 800-2000 frames and $SMOOT_{human\ skin}$ is optimized to process movies of 400 frames.

The color-coded track overviews of the movies made at the eight different locations are shown in Sup. Figure S1. Linear segments are depicted in red, slight turns in blue and sharp turns in yellow. The latter consisted of both SPZ moving forward while turning sharply and SPZ moving back and forth (pendulum movement) making a 180° turn (see also Figure 6 for more detailed explanation of this movement pattern). In the overviews, these tracks seem linear but are coded “yellow”, because of their 180° sharp turn. The movement pattern distribution of the Pf^{WT} and Pf^{RA} was quantified at frame level. In both donors more sharp turns were found in the Pf^{RA} sample. In donor 1, Pf^{WT} did make some sharp turns and one SPZ started circling, while Pf^{RA} made more sharp turns in the form of reversal movement (Sup. Figure S1A-D). In donor 2, the Pf^{RA} exhibited the circling movement, which is observed *in vitro* (Sup. Figure S1G-H). The difference in movement pattern distribution seen for the Pf^{RA} in donor 2 (Sup. Figure S1G-H) revealed the effect of location on movement pattern and underlined that the location needs to be standardized as much as possible by using the same part of the skin and imaging at the same depth.

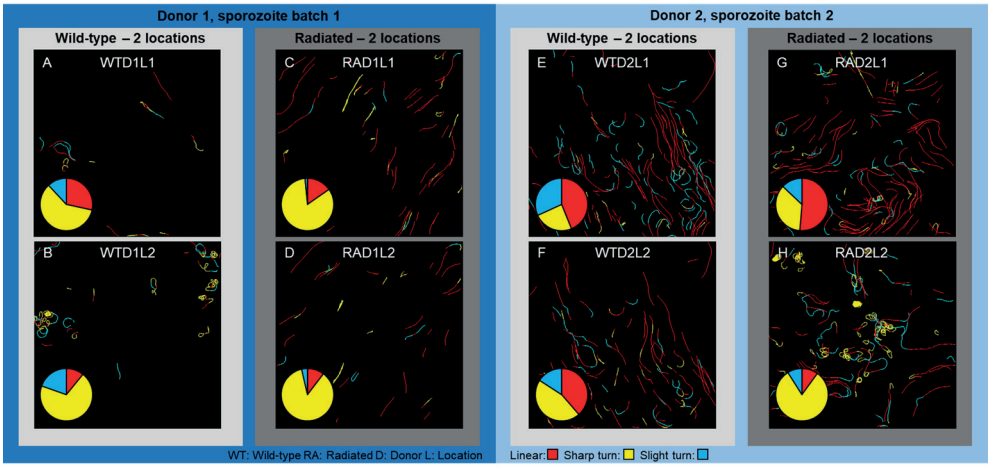

Sup. Figure S1 Overview sporozoite tracks for individual locations. A-B) Track overview and movement pattern distribution for *Pf*^{WT} injected into the skin explant from donor 1 and imaged at two different location. C-D) Track overview and movement pattern distribution for *Pf*^{RA} injected into the skin explant from donor 1 and imaged at two different location. E-F) Track overview and movement pattern distribution for *Pf*^{WT} injected into the skin explant from donor 2 and imaged at two different location. G-H) Track overview and movement pattern distribution for *Pf*^{RA} injected into the skin explant from donor 2 and imaged at two different location. The field of view was 290x290 µm for all movies.

Pooling of individual experiments

The data from the eight different locations was pooled before the detailed motility analysis was performed, which is reported in the main manuscript. Sup. Figure S2 shows the effect of pooling per donor and the effect of pooling the data from both donors. The same trend is visible when comparing the movement pattern distribution of *Pf*^{WT} and *Pf*^{RA} per donor or after pooling the data from both donors.

In vitro assay with *Plasmodium falciparum*

For the *in vitro* assay, the SPZ were obtained in the same way as for the experiments in human skin explants. For imaging of the SPZ, 10 µl of the SPZ solution was pipetted on the cover slip of a confocal dish without any precoating (ø14mm; MatTek Corporation), covered with another cover slip (ø12mm; VWR Avantor) and imaged within half an hour (Sup. Movie 4).

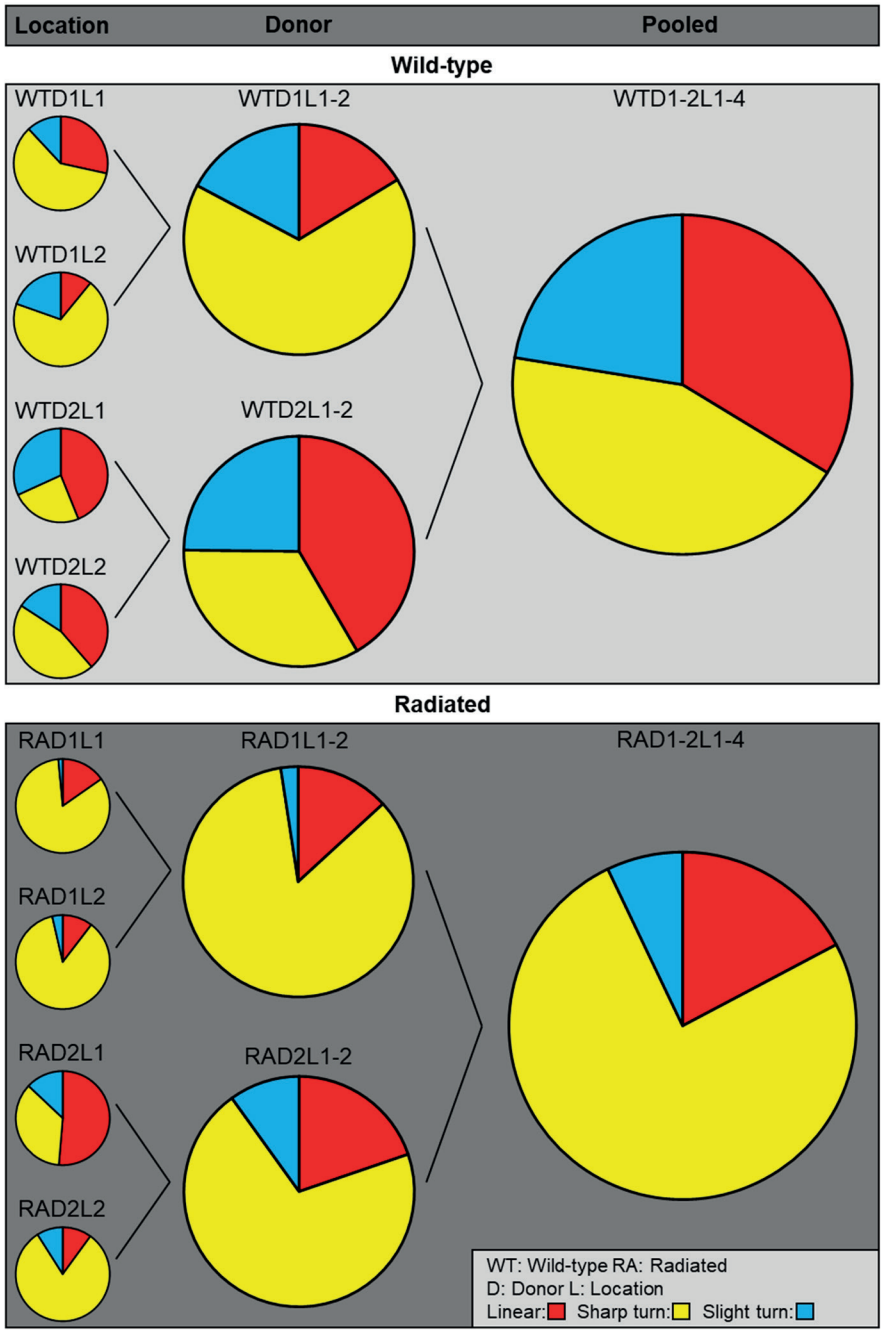

Sup. Figure S2 Pooling process of sporozoite motility data. The movement pattern distribution is shown for wild-type and radiation attenuated SPZ (Pf^{WT} and Pf^{RA}) per individual location (L), per donor (D) and after pooling. The movement pattern distribution of Pf^{RA} was significantly different from the movement pattern distribution of Pf^{WT}, both per donor and after pooling ($p<0.0001$; Chi-Squared test).

Sporozoite velocity and movement pattern distribution over time

To assess the influence of the time on SPZ velocity we longitudinally sampled 1 movie file over a 2 hr time period, see Sup. Figure S3. This data suggested that in the current setting time had little influence on the velocity of *Plasmodium falciparum* (trendline slope: decrease of 0.0023 µm/sec per minute; R^2: 0.3). In the same movie we assessed the influence of time on the turning behavior of SPZ and again, there seem to be little to no influence (trendline slope: decrease of 0.09 percent per min; R^2: 0.4).

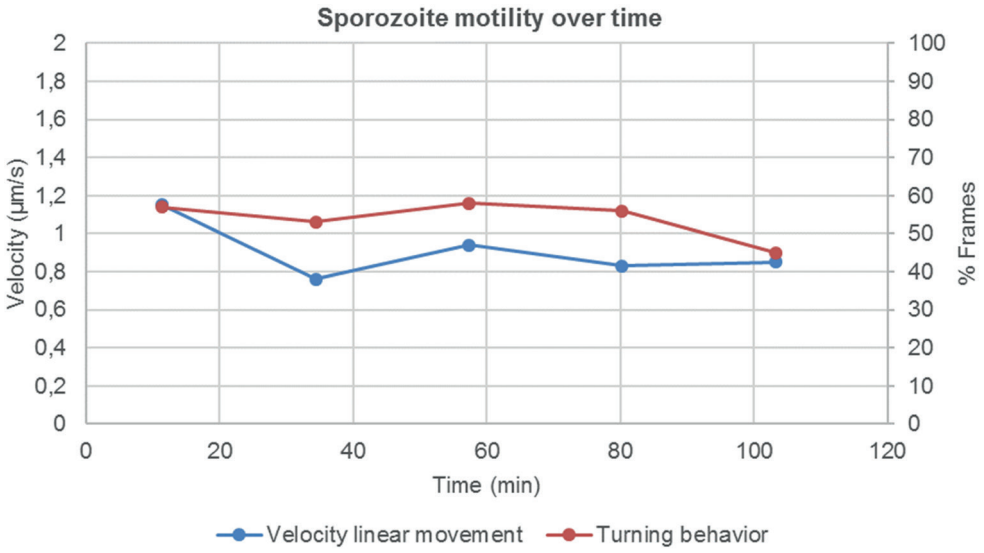

Sup. Figure S3 Sporozoite motility over time. A 4000 frames movie file was longitudinally sampled in 5 sections of 800 frames (23 min). The velocity of the SPZ during linear movement is depicted in blue and the percentage of turns (calculated at frame level) is depicted in red.

Supplementary movies

Movie S1 Example of a confocal microscopy movie showing *Pf*^{WT} migrating through human skin explant tissue.

Movie S2 Example of a confocal microscopy movie showing *Pf*^{RA} migrating through human skin explant tissue.

Movie S3 Example of reversal movement exhibited by *Pf*^{RA}.

Movie S4 Example of *Pf*^{WT} motility on uncoated glass surfaces.

These movies are available online:
http://dx.doi.org/10.1038/s41598-019-49895-3